# DEVELOPMENT OF A TISSUE EQUIVALENT PHANTOM FOR TESTING THE PERFORMANCE OF AN ULTRASONIC HYPERTHERMIA APPLICATOR

BY

PANAYIOTIS HADJIMITSOS

B.Eng., Pratt Institute, 1984

THESIS

Submitted in partial fulfillment of the requirements
for the degree of Master of Science in Electrical Engineering
in the Graduate College of the
University of Illinois at Urbana-Champaign, 1986

Urbana, Illinois

# DEVELOPMENT OF A TISSUE EQUIVALENT PHANTOM FOR TESTING THE PERFORMANCE OF AN ULTRASONIC HYPERTHERMIA APPLICATOR

BY

PANAYIOTIS HADJIMITSOS

B.Eng., Pratt Institute, 1984

THESIS

Submitted in partial fulfillment of the requirements
for the degree of Master of Science in Electrical Engineering
in the Graduate College of the
University of Illinois at Urbana-Champaign, 1986

Urbana, Illinois

# DEVELOPMENT OF A TISSUE EQUIVALENT PHANTOM FOR TESTING THE PERFORMANCE OF AN ULTRASONIC HYPERTHERMIA APPLICATOR

BY

PANAYIOTIS HADJIMITSOS

B.E.E., Pratt Institute, Brooklyn, New York, 1984

THESIS

Submitted in partial fulfillment of the requirements
for the degree of Master of Science in Electrical Engineering
in the Graduate College of the
University of Illinois at Urbana-Champaign, 1986

Urbana, Illinois

# DEDICATION

This thesis is dedicated to the following people for the continuous support and unlimited encouragement that made my graduate studies an invaluable experience well beyond scholarship.

Adamos Adamides

Anderson Ahamad

Cliff Burdette

Iriana Diakidou

Wanda Elliott

Steve Goss

Trudi Fanale

Angeliki Hadjimitsos

Tassos Hadjimitsos

Alexandros Lefkopoulos

Richard Magin

Ann Mannchen

Dave Padgitt

Laura Semerjian

# TABLE OF CONTENTS

# CHAPTER 1

## INTRODUCTION

Hyperthermia cancer therapy is the therapeutic utilization of elevated temperatures to treat tumors [Hahn, 1982]. It is used in combination with chemotherapy and ionizing radiation to increase their clinical effectiveness [Bertino, 1984; Separato, 1979].

Microwaves, ultrasound, or radio frequency currents are used to produce the required heat for localized hyperthermia [Storm, 1983]. Radio frequency heating requires the invasive placement of sources within the tumor. Ultrasound and microwaves are both noninvasive methods, but each exhibits inherent advantages and disadvantages. Ultrasound may be focused but has poor transmission through bone and air. Microwaves are more difficult to focus due to their relatively long wavelengths and have a high absorption coefficient in tissue thereby reducing overall treatment penetration capabilities, but they can be used in the presence of bone and air cavities [Iskander, 1982]. While a number of commercial microwave hyperthermia systems presently are available, ultrasound has only recently been introduced for hyperthermia application.

There are many types of ultrasound applicators that could be used for hyperthermia cancer treatment [Iskander, 1982]. In its simplest form, an ultrasound applicator is a stationary ultrasound source that provides acoustic energy to a fixed volume of tissue according to the energy deposition pattern of the transducer element (fixed applicator). A moving applicator

rotates an ultrasound source to provide energy distribution to a large area. A multielement applicator consists of a cluster of stationary applicators that provide good control of energy deposition over a large area by adjusting the acoustic power of each element. A phased array applicator is the most flexible of all. The ultrasound beam can be focused at a point, and this focal point can be moved in three dimensions electronically by controlling the relative phase of each radiating element.

For hyperthermia to be effective, the temperature within the tumor should be uniform. In clinical situations the temperature variations must be kept within $1^{o}C$ of the selected treatment temperature [Separato, 1982]. Before using an applicator in the clinic, testing procedures to monitor hyperthermia applicator operation and heating effectiveness must be performed. These procedures should include measuring the deposition of ultrasound in a model tissue phantom. Static phantoms and dynamic phantoms have been used to determine the heating patterns of hyperthermia applicators [Cetas, 1982]. Dynamic phantoms, which have a variable liquid flow through them that simulate blood flow, are difficult to fabricate and complex to evaluate. In the present study, a static hyperthermia phantom that measures energy deposition and provides primary quality assurance data was designed, assembled, and tested.

The phantom material employed exhibits sound propagation and static thermodynamic properties similar to that of soft tissue. A matrix of thermocouples embedded in the phantom provided the temperature data needed for determination of the heating pattern. Different heating patterns for a multielement ultrasound

hyperthermia applicator were obtained. Temperature versus time curves permitted measurement of the energy deposition rate and local phantom thermodynamic constants. Specific protocols for the quality assurance testing of ultrasonic applicators were not established. The experimental results showed that the static phantom could be used for the evaluation of hyperthermia applicators. Potential uses of the phantom as a dosimetry system were also explored. It is anticipated that heating patterns of ultrasound applicators can be tested using the static phantom and that the results will aid in the establishment ot controlled, reproducible clinical treatment systems.

Quality assurance methods that test the effectiveness of hyperthermia applicators are very much needed. The complexity of equipment and the principles of operation of hyperthermia systems do not allow for standardized, easy to make measurements that would determine the operational status ot the equipment. A simple method that gives reproducible data and directly tests the final stages of hyperthermia systems would be useful. The quantification of the applicator heating performance allows periodic comparisons for the same unit or for a group of units. This type of testing will assure that optimal therapeutic performance can be obtained.

# CHAPTER 2

# EXPERIMENTAL PROCEDURES

## 2.1. General

### 2.1.1. Measurement and Instrumentation

There are a variety of parameters needed to determine the safe and effective operation of a hyperthermia system. Proper results for one parameter do not guarantee the proper operation of the whole unit. Some of the important parameters that are commonly tested are now described.

The acoustic intensity generated by each transducer element of an ultrasound hyperthermia applicator is the most important factor, since it determines the power absorbed by tissues and the degree of heating. The more power per unit area from an element, the faster it will heat a given volume of tissue, i.e., the higher the resulting temperature will be for a fixed amount of time. Therefore, in the absence of rapid heat loss, the rate of temperature rise may be used to determine absorbed power.

The uniform energy deposition by an element is very important. A way to test for uniformity of energy deposition is to measure the beam plots of each element. Large peaks and troughs detected in the beam plot indicate nonuniform energy deposition. The temperature peaks obtained in a transverse direction across the applicator, or in the longitudinal direction away from the applicator face, are quantifiable factors describing the ultrasonic beam.

The depth of penetration is also an important parameter to determine in establishing the effectiveness of the hyperthermia applicator in treating deep-seated tumors. The depth of penetration is dependent upon the frequency of the incident ultrasonic energy and the absorption properties of the tissues in the acoustic path.

The following experimental equipment is needed to determine the performance characteristics of an ultrasonic hyperthermia applicator: a power source, a tissue mimicking material instrumented with temperature sensors, a positioning system, and a temperature recorder/analyzer. The power source provides the necessary high intensity ultrasound energy. The tissue mimicking material absorbs the ultrasound energy and converts that energy into heat that is detected by a series of embedded thermocouples. The temperature recorder/analyzer measures the temperature patterns and extracts the information needed to quantify the hyperthermia performance characteristics of the source. The positioning system provides in-position-dependent measurements such as the spatial distribution of the energy in the heating beam.

### 2.1.2. Methods Previously Used for Ultrasound Hyperthermia Measurements

Power measurements have been made using the radiation force technique and a method in which thermocouples are embedded in an ultrasound absorbing material [Repacholi, 1981]. Beam plots have been obtained with hydrophone probes and moving thermocouples in water and oil tanks. Depth of penetration measurements have been

made using *in vitro* tissues, and in tissue phantoms with thermocouples inserted at various depths [Lele, 1983].

### 2.1.3. Difficulties of Previous Methods for Hyperthermia Quality Assurance

These previously used methods are not suitable for hyperthermia quality assurance because they provide fractionated information. Each method requires its own specially designed and dedicated apparatus. Most of the methods are time consuming and provide results in a format not useful for medical personnel. Finally, because of the variety of ways the same method has been used, the repeatability of the measurement is difficult to establish.

A well designed quality assurance system for hyperthermia applicators should use existing equipment. The results produced should be in a readily comprehensible quality assurance format covering such parameters as beam plots, specific heat power deposition, depth of penetration, absorption, and heat diffusion.

In this study, a tissue-mimicking phantom with embedded arrays of thermocouples, a multichannel temperature measurement device, and a microcomputer for data processing are used to investigate the measurement of performance factors of ultrasonic hyperthermia equipment. The phantom was positioned in a water tank. Such a system can perform power, depth of penetration, and beamwidth measurements. It is anticipated that this test system could be scaled down and simplified for routine use in clinical hyperthermia therapy programs.

## 2.2. Instrumentation

### 2.2.1. General

A variety of existing equipment at Labthermics Technologies, Inc., Champaign, Illinois was assembled to test the instrumented tissue phantom concept for quality assurance of ultrasound hyperthermia systems (Fig. 2.1) (all figures appear after the text). The phantom was designed and manufactured according to specifications that enable measurement of the important ultrasound hyperthermia performance parameters. For the power source and the thermometry a SONOTHERM 1000 multichannel clinical hyperthermia system was used. The SONOTHERM 1000 is a complete ultrasound hyperthermia system consisting of an ultrasonic applicator, an acoustic power generator, a thermocouple thermometer, and a minicomputer for control. In addition, an Apple IIe microcomputer was used for high speed temperature data logging and analysis. The spatial positioning of the applicator and the phantom was obtained using an ultrasound scanner [Padgitt, 1984] for position-dependent measurements.

### 2.2.2. Instrumented Tissue Phantom

#### 2.2.2.1. Design Criteria

The size of the phantom was determined with consideration of large and small ultrasonic hyperthermia applicators. A small phantom would not be able to measure the heating patterns of a large applicator. On the other hand, a large phantom would provide data of limited accuracy for a small applicator. A trade off was required, and a large phantom, 28 cm by 28 cm by 8.9 cm

was chosen. The number and position of the thermocouples were determined next.

The initial design consisted of 64 thermocouples arranged in a cubic lattice. The cube would have four parallel planes each having 16 thermocouples arranged in a square, four by four array. This thermocouple arrangement allows power, power distribution, and penetration depth to be measured. However, the large number of thermocouples greatly increases the complexity of manufacturing the phantom, and the additional amount of data obtained would not significantly increase the resolution of the heating pattern.

Because of these factors, a reduced version of the cubic lattice scheme shown in Fig. 2.2 was adopted. Two of the four planes were implemented. The two planes intersect each other and require a total of 28 thermocouples.

The phantom is made water submersible, with acoustic windows placed on each side to alleviate standing wave fields that would compromise the measurements. A degree of portability is incorporated in the design. There is a bracket that allows mounting the phantom in a holder or spatial positioner and the thermocouples are terminated in special copper constantan plugs that mate with connectors on the thermometry face. Protective side covers for the phantom allow storage and transportation.

2.2.2.2. Filling

The Plexiglas frame of the phantom is filled with a material that mimics the ultrasound and thermal properties of human tissue. The filling is a graphite-agar-alcohol mixture. The

mixture was developed and produced by Dr. James Zagzebski at the University of Wisconsin. The acoustic properties of the mixture are given in Table 2.1.

2.2.2.3. Thermal Expansion and Structural Strength

The thermocouples must be able to withstand thermal expansion or contraction and still maintain their relative position. The phantom structure needs to be strong for portability and repeatability of the tests. Plexiglas walls of 6.35 mm thickness were used. Plexiglas has a low coefficient of thermal expansion, and at this thickness is relatively strong.

2.2.2.4. Construction

The Plexiglas structure was machined to a high precision to guarantee a tight fit of the Plexiglas walls and a good geometry. The geometry of the phantom was very important for the thermocouple junctions.

The thermocouple junctions were formed with bare copper and constantan wire. Constantan wire of 0.127 mm in diameter was used as a bus for the thermocouple junctions. Copper wire of 0.762 mm diameter was wrapped around the constantan bus once for each junction. Low temperature melting fine mesh soldering cream (Alloy 60/40, mesh 325 Type P-327, by Kester, Chicago, IL) was applied and melted in place using a heat gun instead of a soldering gun to avoid breaking the fine copper wire due to excessive heating. One end of the copper wire was then cut off. The other side formed a thermocouple. Each thermocouple bus was terminated at the wall of the phantom, where a higher gauge thermocouple wire strain relief was employed for additional

strength. To prevent electrical short circuits, the thermocouple wire was coated with three layers of clear lacquer nail polish.

The phantom was filled with the acoustic phantom material by Dr. Zagzebski's group at the University of Wisconsin.

All thermocouple junction resistances were recorded before shipping the phantom for filling. After receiving the filled phantom the resistances were recorded again. One thermocouple bus (four junctions) was damaged during the filling process. The remaining junctions maintained the same resistances, indicating low corrosion and viable junctions.

### 2.2.3. SONOTHERM 1000

The SONOTHERM 1000 is a commercial ultrasound hyperthermia system. The system is normally computer controlled, and it operates with a 16 channel thermometry system (TX-100). For testing the operation of the acoustic tissue phantom, the SONOTHERM 1000 was set up for manual operation, using an ASCII terminal to communicate with the on-board microprocessor controller.

### 2.2.4. Data Acquisition

The TX-100 was connected to an Apple IIe personal computer. A John Bell Parallel Interface Card (John Bell Engineering, Redwood City, CA 94064) provided the necessary interface between the serial port of the TX-100 and the parallel port of the Apple IIe computer.

### 2.2.5. Required Hardware

A 153 liter water tank was filled with hot water and allowed

to degas for two days before testing. A three-dimensional positioning system [Padgitt, 1984] was manually operated to position the phantom inside the water tank in a precise, reproducible manner relative to the ultrasound applicator.

## 2.3. Procedures

### 2.3.1. Types of Measurements

#### 2.3.1.1. Beam Plots

The beam plot measurements are the most difficult to make because of the time and effort involved in data collection and interpretation.

The phantom is moved in front of the applicator in equal increments for a total length equal to the width of two transducer elements. At each position the ultrasound power is turned on for a fixed amount of time. The final temperature at the end of this interval is used to form a plot of temperature versus distance. The magnitude of the acoustic intensity as measured by the rate of temperature rise is expected to be at a relative maximum over the distance roughly equal to an element's width and drop off sharply outside this region.

#### 2.3.1.2. Depth of Penetration

The depth of penetration measurements are obtained in a straightforward manner. A diagonal plane of thermocouples is selected and the ultrasound energy is applied for a fixed time. The peak temperatures reached at different depths are compared to determine the extent to which heating at depth is achieved.

2.3.1.3. Rate of Temperature Rise

The rate of the temperature rise in the phantom is the most general type of measurement that can be obtained. Because all quality assurance measurements discussed here involve heating the phantom with ultrasound energy for some time, the result is a set of curves of temperature rise versus time which may vary according to the relative spatial position of the phantom and applicator, or with depth. These temperature rise slopes can be used to determine absorption and specific heat for the phantom material. The cooling characteristic of the phantom could be used to determine other thermodynamic properties of the phantom such as heat diffusion rates.

2.3.1.4. Absorption and Specific Heat

Absorption and specific heat are calculated from the slope of the temperature rise curves. They are used to verify the acoustic and thermal properties of the phantom. The equations used for the calculation of these parameters are given in Chapter 3.

2.2.2. Measurement Protocol

2.3.2.1. Hardware

The water tank is filled with warm or hot water (hot water contains less dissolved oxygen than cold water) and is left to degas for a couple of days. Next the water tank is lined with sound absorbing material to eliminate standing waves. The phantom is mounted on the positioner and submerged in the water. At the time of the mounting, the side of the phantom that will face the applicator is chosen. Different positions of the

thermocouples with respect to the applicator can be obtained from the two sides. The applicator's head is filled with degassed water and positioned on top of the phantom. A careful visual alignment of the applicator with respect to the four corners of the phantom is very important for a valid data acquisition. Each of the thermocouples is constructed in such a way as to be at the center of each of the 16 elements of the ultrasound applicator. The exact alignment of the applicator's head is most important for the beam plots. The thermocouple leads are then connected to the TX-100, the thermometry system. The SONOTHERM 1000 is configured for external manual control of intensity and ultrasound patterns. The TX-100 is connected to an Apple IIe microcomputer for data recording.

2.3.2.2. Thermal Equilibrium Check

All the different experimental procedures require the measurement of temperature differentials versus time. The quality of the data obtained is directly related to the accuracy and validity of the recording of the temperature differences.

The phantom can be heated in at least two ways. The most obvious is by irradiation by ultrasound energy. The least obvious is by heat conduction. If some regions of the phantom are heated to higher temperatures than the rest of the phantom, heat will diffuse from the regions of high temperatures to those of lower temperatures. Thus, during an experimental run with a phantom that is not at thermal equilibrium, the recorded temperature differences are the result of irradiation and heat conduction. The thermal equilbrium is checked in the following

way. The median temperature of the 16 thermocouples is chosen as the reference temperature for the different display modes. All the other temperature readings are now higher or lower than the median. An experiment can only be carried out when none of the thermocouple readings vary more than half a degree Celsius from the median to prevent significant temperature reading errors due to heat flow.

2.3.2.3. Power Application and Data Recording

One minute of data for each of the 16 thermocouples is recorded prior to the application of power. This provides enough time for manually setting the ultrasound control for the SONOTHERM 1000, both the number of elements that will be on and their levels, and provides verification of thermal equilibrium. The applicator power is then applied to the phantom for a duration of one to three minutes. This length of time has been shown to be adequate for data recording without overheating the phantom. The power is then shut off and temperatures are recorded for additional time to observe the cooling characteristics of the phantom. This cooling time can also be used for establishing thermal equilibrium of the phantom.

The fastest data recording rate is one set of data for each of the 16 thermocouples every two seconds. This limitation is due to the limited transfer rate of data from the Apple IIe memory to diskette. At the end of the experiment the temperature distribution of the phantom is monitored until a thermal equilibrium is established and a new experiment can be started.

#### 2.3.2.4. Data Plotting and Interpretation

Each experiment creates a data file of sequentially recorded temperature readings. From this file, individual files for each thermocouple are created. The data for each thermocouple are plotted as a temperature versus time plot. This type of plot is used for all subsequent analyses. The amount and type of information extracted from these plots depend on the depth and position of the thermocouples as well as the power level.

## 2.4. Details of Different Types of Measurements

### 2.4.1. Slope Measurements

All the measurements provide rate of temperature rise information. This rate information can be used for comparing individual elements of the applicator. Knowing the specific heat of the phantom material and taking into account the heat diffusion rate, the actual power delivered can be determined.

### 2.4.2. Depth Measurements

Depth measurements are achieved by selecting thermocouple busses of different depths and by irradiating all of them with equal power.

### 2.4.3. Beam Plots

Beam plots are obtained by repeating the same heating pattern at different predetermined spatial positions of the phantom under the applicator. An interval of one tenth of an inch was chosen and 20 sets of measurements were made. The phantom is positioned in such a way that the thermocouple is one inch away from the symmetry axis of the element. At the tenth

measurement the thermocouple is at the center of each ultrasound transducer element. This pattern is followed so that the effect of adjacent elements can be evaluated.

### 2.4.4. Absorption Measurements

Absorption measurements are made by relating temperature data at different depths.

## 2.5. Data Presentation and Error Analysis

### 2.5.1. Temperature Versus Time Plots

These plots are the basis for all information extracted for each type of measurement. Slopes are calculated from these plots as the rates of temperature versus time. The peak temperatures reached are used in depth, beam plots, and absorption measurements.

### 2.5.2. Peak Temperature Tables

The peak temperature tables show the peak temperatures reached at the end of the irradiation time. They provide information on the depth of penetration and the acoustic absorption of the materials if the incident power and thermal characteristic of the material are known. The acoustic absorption of the material is tabulated in the power deposition tables.

### 2.5.3. Beam Plots

The beam plots are obtained by plotting the peak temperatures versus position of the instrumented phantom relative to the applicator face.

# CHAPTER 3

# RESULTS

## 3.1. Overview

Several sets of data were collected using the methods described in Chapter 2. Following acquisition, the data were manipulated to extract the specific information pertinent to the type of measurement. Data were analyzed in order to obtain beam plots, specific heat of the phantom material, power deposition, depth of penetration, acoustic absorption, and heat diffusion.

The heat diffusion measurements illustrated the heat transfer from radiated to nonradiated regions of the phantom. The specific heat of the phantom material was calculated experimentally and compared with the design value. The experimentally determined specific heat was used in all subsequent power deposition measurements. The absorption measurements were compared with the theoretical values to determine the validity of the phantom's material attenuation coefficient. The depth of penetration measurements determined the ultrasound energy attenuation at various depths. Beam plots provided the axial temperature distribution for each element. The overall temperature distribution due to a row of elements was also assessed. In addition, beam plots were made for various depths in the phantom.

The important information from the various experimental runs was summarized in tables or plots. Only in cases where actual

numerical values of temperature data are needed to illustrate a point are such values provided again in a table format.

## 3.2. Specific Heat

The rate of temperature increase data was used to calculate the specific heat of the phantom material. The calculated specific heat was used subsequently in all power deposition calculations. The temperature versus time data are given in Table 3.1 and the plot of this data is given in Fig. 3.1.

The temperature rise versus time curves of each thermocouple for all experimental runs were carefully reviewed to obtain the data needed to calculate the specific heat of the phantom material. The criterion used to single out one data set from the many available was the linearity of temperature rise versus time. Such a situation is not typical. A linear temperature rise for more than a few seconds indicates improper heat conduction. The material is using all the absorbed energy to raise its temperature. Typically the material conducts heat to adjacent nonirradiated areas. A typical temperature rise versus time curve is given in Fig. 3.2.

## 3.3. Specific Heat Calculation

The equation used to calculate the specific heat of the materials employed in the experiments was derived from the Bioheat Equation [Bowman, 1975], Eq. (3.1)

$$K\nabla^2 T + \omega C_b(Ta-T) + \dot{q}m + P = \rho c(dT/dt) \qquad (3.1)$$

In Eq. (3.1) the first left term, $K\nabla^2 T$, accounts for the heat diffusion, the second term, $\omega C_b(T_a-T)$, accounts for the blood

perfusion, the third term, $\dot{q}m$, accounts for metabolism, and the fourth term, P, accounts for the ultrasound source power in $W/cm^3$. The only term on the right side, $\rho c(dT/dt)$, gives the temperature change with respect to time for a material with a known density and specific heat.

The specific heat calculations were made with minimum existing temperature differentials thus the first term is set to zero. The phantom material has no perfusion capacity or metabolic activity, thus terms two and three are set to zero. The resulting equation is

$$P = \rho c \ (dT/dt) \tag{3.2}$$

Equation (3.2) shows that the power absorbed per cubic centimeter of material equals the density of the material times its specific heat times the rate of temperature increase with respect to time. Rearranging the terms of Eq. (3.2) results in Eq. (3.3)

$$C = \frac{P}{\rho \ (\frac{dT}{dt})} \tag{3.3}$$

Equation (3.3) indicates that given the power absorbed per $cm^3$ of material, its density, and the change of temperature rate, the specific heat of the material can be calculated. The value of the term P can be the power difference $P_A - P_B$ calculated using Eq. (3.5) with $d_{AB}$ = 1 cm and incident powers expressed in Watts per $cm^2$.

The specific heat was calculated using the data in Fig. 3.1. It was found to be 3.386 $J/cm^3$ for this case of a linear increase in temperature.

## 3.4. Beam Plots

The beam plots were used to determine the final temperatures reached along the axis of transducer elements. The beam plots were used to determine the effectiveness of the elements in heating areas of the phantom uniformly. The beam plots for 12 thermocouples at different depths are given in Figs. 3.3, 3.4, and 3.5. Large temperature variations were observed in most of the recorded beam plots.

The beam plot data were collected by the repeated application of ultrasound to the phantom as it was moved transversely in equal increments of distance. A total distance of 5.08 cm was covered in steps of 0.254 cm. Initially, the phantom was offset by 2.54 cm from the on axis center. The thermocouple coincided with the element's axial center only during the eleventh irradiation (see Fig. 3.6 for the offset distance set up). Each irradiation lasted 30 seconds. After the irradiation the phantom was moved to the next position and a 20 minute cool off interval was observed. The quantifiable parameter in the beam plot experiments was the final temperature reached at the end of the 30 second interval.

## 3.5. Power Deposition

The measurement of power deposition was used to evaluate the performance of each of the applicator's elements. The equation used for the calculation of power deposited is given in the next section of this chapter.

The power deposited about the volume of each of 16 thermocouples arranged in a 4 x 4 grid at a depth of 2 cm is

shown in Tables 3.2, 3.4, and 3.6 for three sets of data. Irradiation lasted for 60 seconds. The final temperatures reached at the end of the 60 second period for each of the data sets are shown in Tables 3.3, 3.5, and 3.7. Detailed information about the experimental conditions for each of the three runs is provided in Figs. 3.7 through 3.9.

## 3.6. The Attenuation Equation

The power equation, Eq. (3.4), was used for the theoretical calculation of the attenuation of acoustic power at different depths of a material with an attenuation coefficient $\alpha$.

$$d_{AB} \cdot \alpha = 10 \log_{10} P_A/P_B \qquad (3.4)$$

In this equation the attenuation coefficient is given in dB/cm and accounts for both the absorption and scattering of ultrasound. The power at point A is $P_A$ and $P_B$ is the power at point B. The distance between points A and B is $d_{AB}$, where points A and B lie along the axis of propagation for the ultrasound wave. Knowing the incident power at point A and the attenuation coefficient $\alpha$ (a function of the material and the irradiating ultrasound frequency) and given the distance between points A and B, the power at point B can be found. Rearranging Eq. (3.4)

$$P_B = \frac{P_A}{10\left(\frac{\alpha - \alpha_{AB}}{10}\right)} \qquad (3.5)$$

The power differencee $P_A - P_B$ gives the amount of power absorbed and scattered by the material lying between points A and B. If

the power absorbed by the material is known, then the difference between the attenuated and absorbed powers equals the scattered power.

## 3.7. Depth Penetration and Absorption

The power deposition at different depths provides an estimation of the depth of penetration. Depth of penetration was used to determine the effectiveness of the transducer elements in heating volumes well below the surface of the phantom material.

The power deposited and the final temperature reached at 60 seconds as a function of depth are given in Tables 3.8 and 3.9. The set up is described in Fig. 3.10. Power measurements were indirectly made to verify the absorption coefficient of the phantom material.

The attenuation equation, Eq. (3.4), was used to determine the ultrasound power as a function of depth. The difference of powers at two different depths on the same perpendicular line equals the amount of power absorbed and scattered. This amount of power is tabulated in Table 3.10 and compared with data from Table 3.8 in Table 3.11.

## 3.8. Heat Diffusion

The heat diffusion data were used to determine the effect of heat transfer to a nonirradiated area from the irradiated area. Two sets of data were obtained: the first with the inner four elements of the transducer active on, and the second with the outer 12 elements active on. The power deposition for the outer 12 elements and the final temperatures reached at 60 seconds for 16 thermocouples at a depth of 4 cm are tabulated in Tables 3.12

and 3.13. Detailed information for the experimental set up is provided in Fig. 3.11. The power deposition and the final temperatures reached when the four inner elements were active are shown in Tables 3.14 and 3.15. Detailed experimental set up information is given in Fig. 3.12.

## 3.9. Quantification of the Thermometry System

### 3.9.1. Noise

The initial sets of data were affected by a noise problem in the thermometry system. The noise was in the form of a temperature waveform with a period of 5.5 sec and an amplitude of $\pm$ 0.08$^{o}$C. The resulting data contained the noise superimposed on the recorded temperature rises as shown in Fig. 3.13. The first 10 sec of experimental data were of great importance. Thus, a comparison of actual data and noisy data is given in Table 3.16. The data used were extracted from Fig. 3.13. Averaging the sampled data over a period of 10 sec given a slope of 0.0455$^{o}$C/sec, a 5% error over the actual 0.5$^{o}$C/sec value. Thus, the calculation of the slope of the temperature rise is not significantly affected by the noise.

### 3.9.2. Thermocouple Testing Procedure

Fine copper and constantan wires of 0.0762 mm and 0.127 mm, respectively, in diameter were used in the construction of 28 thermocouples. Because of their small size, regular impedance checks of the thermocouple wires were made to detect break or deterioration due to corrosion. During the first test, a variation of $\pm$ 4% was detected. This amount and type of variation were decided to be critical. A close examination of

the resistance measurements revealed that the resistance fluctuations were due to a procedural error. In Fig. 3.14 the physical circuit as well as the two possible equivalent electric circuits involved in a resistance measurement are shown. The thermocouple is modeled as a voltage source in series with a resistance. The polarity of this voltage source is the source of an apparent error in resistance values of $\pm$ 4%. This source of error is eliminated by choosing to measure the thermocouple resistance by applying the red lead of the multimeter on the copper end and the black lead on the constantan end.

# CHAPTER 4

# DISCUSSION

## 4.1 Introduction

The experiments performed on this project were designed to develop and evaluate methods for analyzing the absorption of acoustic energy in an ultrasonic phantom. The details of the methods are described in Chapter 2, and the results are tabulated in Chapter 3. The procedures allowed the collection of a large amount of experimental data. This data was subsequently analyzed and used to characterize the performance of the ultrasonic hyperthermia applicator and the ultrasonic phantom. Some problems with the experimental set up and the data collection procedure were not recognized until well after the experiment was over. This occurred because data had to be collected at one time and analyzed at another. Rectifiable problems of this nature, e.g., air bubbles on the applicator's surface, were detected only when the data was analyzed. Other problems, e.g., the fluid thermodynamic properties of the tissue simulating phantom, proved to be very complicated and difficult to analyze.

The project's initial goal was to establish clinical testing procedures for ultrasound hyperthermia applicators. This goal was not met due to the qualitative nature of the experimental results. A more rigorous understanding of the phantom's properties and behavior is needed before a protocol for routine testing can be established.

Since the interpretation of the results depends on the confidence one has in the quality of the data, an extended discussion of each experiment's results and the problems encountered follows. In addition modifications to the phantom or measurement procedures that would improve the system are suggested.

4.2.1. Specific Heat

The slow rate of data acquisition and the low acoustic power applied on the phantom made the determination of specific heat very difficult. All temperature versus time plots were carefully reviewed to select curves that clearly approximated a straight line for an extended period of time. Most of the plots were clearly of an exponential nature indicating that the heat was immediately carried to adjacent regions by heat conduction. The plot selected to calculate the specific heat, Fig. 3.1, was obtained from a thermocouple located at the center of the irradiated area closest to the applicator's surface. At this location the thermal conduction should be minimal. A more typical plot of temperature rise versus time is shown in Fig. 3.2 where the effects of heat conduction are clear. The determination of the specific heat from this type of experiment is indirect and only provides a secondary check of other determinations. The value obtained, 3.386 $J/cm^3/^oC$, is close to the value of 3.595 $J/cm^3/^oC$ reported by Dr. James Zagzebski for this type of phantom material. In subsequent power absorption calculations, the value 3.386 $J/cm^3/^oC$ for the specific heat was used.

4.2.2. Beam Plot

This measurement was greatly affected by the presence of air pockets on the applicator's surface. Air pockets were created while the experiment was running. The air dissolved in partially degassed water accumulated in air cavities created by the ultrasound. The beam plots of locations 7D through 7A and 4D through 4A, as shown in Figs. 3.3 and 3.4, were obtained for thermocouples residing on the side of the phantom where most air pockets were discovered. The effect of the air pockets is to destroy the expected acoustic field pattern. This resulted in inconsistent beam plots which could not be analyzed. In the plots of locations 1B and 5B, Fig. 3.5, a typical expected beam plot can be seen. The transducer's 3 dB temperature profile deducted from these two plots, 3.8 cm, is comparable to the 3 dB power beamwidth, 3.1 cm, experimentally determined [Underwood, 1986].

Air pockets could be avoided by using thoroughly degassed water. A problem that cannot be easily overcome with beam plots is the length of time involved. For a 21 point beam plot, a minimum of 11 hours of power application, data collection, and cool off period cycles is required.

4.2.3. Power Deposition

Three sets of data were collected for the power deposition experiment. All three runs used the same experimental set up. Set A, Table 3.2, gives the power deposited for an incident power density of 2.69 $W/cm^2$ and sets B and C, Tables 3.4 and 3.6, for an incident power density of 4.04 $W/cm^2$.

A careful comparison of the three sets reveals that certain regions of the phantom heat faster than others. It is clear that the four center thermocouples 3C, 3B, 2C, and 2B heat the slowest while the four corner thermocouples 4D, 4A, 1D, and 1A the fastest. The results are consistent with the fact that the power deposited at the center of the phantom is lower than the power deposited at the corners. At the eight remaining positions, 4B, 4C, 3A, 2A, 1B, 1C, 3D, and 2D, power deposition values fall between these extremes.

The locational variability of power absorption was attributed to reflected ultrasound waves. Scattered ultrasound would be greatest at the four corners of the phantom (locations 4D, 4A, 1D, and 1A), where the fastest temperature rises are observed. It should not be reflected at all at center locations 3C, 3B, 2C, and 2B (no walls), where the lowest temperature elevations are seen. The problem caused by reflected ultrasound is that it irradiates the same locations more than once resulting in an apparent high power deposition. A solution to the reflection problem would to be use rubber walls on a Plexiglas or stainless steel frame for the construction of the phantom. However, the positional accuracy of the thermocouples may have to be compromised in such a device.

From a careful comparison of locations in the phantom, it is clear that certain locations in the phantom recorded consistently higher power depositions than other locations. Location 4D recorded the highest power deposited in all three sets of experiments. Locations 3B and 3C recorded the lowest power depositions in these three data sets. These observations are

attributed to inhomogeneity in the phantom material and to small variations in the power output of each element of the applicator. The power output of each element was not monitored individually. The total power was divided by the number of elements that were active to determine the power delivered to each element. Output power variations of + 15% for individual elements are described by the applicator's manufacturer.

The percentage of scattered power for data sets A, B, and C are given in Table 4.1. The highest percentage of scattered power is shown in set B, Table 3.4. As was mentioned previously, this high value is due to the presence of air pockets. Thus, the exact numerical value of the scattered power may be higher or lower depending on the particular location. For the percentile calculation, only the average power deposited figures were used and the standard deviation was as high as one-third of the average. Again, the effects of air pockets and of potential acoustic impedance mismatches due to phantom material inhomogeneity are clear.

### 4.2.4. Depth Penetration

The theoretical power deposition for ultrasound at a frequency of 1 MHz as a function of depth is given in Table 3.10. The experimentally determined power depositions for the same depths are tabulated in Table 3.8. The data in Table 3.8 indicate that little or no attenuation of the ultrasound power takes place as the ultrasound penetrates deeper into the phantom. At a depth of 2 cm the power deposited is equal or higher than at a depth of 1 cm. A comparison between power deposited at 5 cm

and at 2 cm indicates an attenuation of 25%, less than the expected theoretical value of 36%.

Experimentally determined power depositions are subtracted from the theoretical calculations and the difference is expressed as a percentage of scattered power in Table 3.11. The percentage of scattered power is higher at shallow depths than it is at deep depths. This increased percentage of scattered power at shallow depths may be due to strong wall reflections.

### 4.2.5. Heat Diffusion

The tabulated power depositions for the 12 outer and four inner elements are given in Tables 3.12 and 3.14, respectively. The previously discussed results of preferential heating due to location with the phantom can also be seen in these results.

Attempts to make a thermodynamic model of the phantom introduced the following complexities. Water removes heat from the exposed surface of the phantom due to heat convection. Heat is also removed from the Plexiglas walls due to heat conduction and from the Plexiglas walls into the water due to heat convection. The adjacent nonirradiated phantom regions also remove heat due to heat conduction. For these reasons the heat diffusion data could not be interpreted quantitatively. Thus, no value for heat diffusion was determined.

The outer 12 and the inner four elements, Tables 3.12 and 3.14, display an average power deposition of 0.108 $W/cm^3$ and 0.80 $W/cm^3$, respectively. This is a small difference. On the contrary, the average temperatures reached at 3 minutes are 3.28$^oC$ for the outer 12 elements, Table 3.13, and 1.79$^oC$ for the

inner four elements, Table 3.15. Heat conduction and convection are proportional to the temperature difference between the two regions of concern. Thus, during the initial period of ultrasound irradiation, most of the absorbed energy increases the temperature of the phantom material. Power deposition calculations are based on temperature versus time data collected during the first few seconds of the experiment. As time progresses, the temperature difference between irradiated and nonirradiated material as well as the surrounding water increases and an increased portion of the heat is carried through convection or conduction to adjacent cooler material. Temperatures at the end of the 3 minute irradiation reflect this fact. Unfortunately, no simple relationship exits between the absorbed power and the temperature at the end of the 3 minute time period because thermal equilibrium has not been established and the flow of heat has not reached a steady state.

A possible solution that may help determine the constant of heat conduction for the phantom material is described below. A single element of the applicator irradiates with very low power ultrasound only one thermocouple situated at the center of a 3 by 3 thermocouple array, e.g., 2D, 3D, 4D, 2C, 3C, 4C, 2B, 3B, and 4B. After a few minutes of irradiation, thermal equilibrium will be established. Thus, all heat resulting from irradiation will be transferred to adjacent material while the thermocouple will maintain a steady temperature. The temperature difference between irradiated and nonirradiated regions can then be recorded. The water interfaces in this situation can be modeled as infinite sinks of heat using the initial water temperature.

Thus, for this experimental situation, the recorded temperature differences can be simply inserted into the steady state solution of the heat diffusion equation to obtain the heat diffusion constant.

## 4.3. Generic Problems

The difficulties created by the use of low power levels and long recording intervals are explained below.

### 4.3.1. Low Power Levels

Low power levels generated problems in the initial sets of data because of the presence of noise of comparable amplitude to the signal level. Although the noise was mathematically modeled and compensated for in the data analysis, higher power levels might have produced power deposition results closer to that indicated by the theoretical calculations. Higher power levels could also give results that are more consistent with the linear approximation calculation for power deposition.

### 4.3.2. Long Recording Intervals

The configuration of equipment used allowed, at best, recording of one set of data readings for all 16 thermometry channels every 2 seconds. For the determination of power deposition, data collected during the first 2 to 4 seconds were the most critical. After the first 2 to 4 seconds, the curve of temperature versus time is no longer linear. Thus, a higher sampling rate for the thermometry system is needed.

# CHAPTER 5

# CONCLUSIONS AND SUGGESTIONS

## 5.1. Conclusions

An ultrasound phantom and associated temperature sensing instrumentation were developed to study the ability of a multielement ultrasonic hyperthermia applicator to deposit heat in a localized region. The thermal characteristics of the phantom material were measured and preliminary studies using a 16 element applicator were conducted. Based on the results of these studies, the following conclusions can be made:

1. The specific heat of the phantom material was determined and found to be in agreement with the design value.
2. The complexity of the heat diffusion dynamics prohibited the determination of the thermal diffusion constant.
3. The power deposition for various configurations of the radiating elements was calculated and the results used to examine the penetration depth of ultrasound at 1 MHz. Due to reflections of ultrasound, the measured penetration depths did not agree with the theoretically predicted values.
4. The use of beam plots in evaluating the temperature profiles of an ultrasound element was demonstrated despite the errors introduced by air pockets present in the applicator's coupling bolus.

## 5.2. Suggestions for Future Studies

### 5.2.1. Power Levels

The power levels used in the experiments were in the range of 2 to 4 $W/cm^2$ of incident power. Both lower and higher power levels must be tried in order to understand the thermal dynamics of the phantom and to determine the heat flow constants. Higher power levels will also help determine the tolerance of the phantom for high energy levels. Absolute temperatures need not exceed $50^oC$.

### 5.2.2. Thermometry Sampling Rate, Accuracy, and Precision

The determination of the power deposition per $cm^3$ of the phantom mass is based on an approximation. This approximation states that for low temperature differentials all the ultrasound energy absorbed is used to raise the temperature of the irradiated mass. As the temperature of the irradiated mass increases, heat flows to adjacent cooler masses. A thermometry system with a sampling rate of 10 or more samples per second and an accuracy and precision of $0.01^oC$ is needed to record enough reliable data points before the effects of heat diffusion dominate. In addition, only short time periods on the order of 5 to 10 seconds will be needed for the experiment thus allowing shorter cooling off intervals. This will increase the rate at which data on applicator performance can be obtained.

### 5.2.3. Real Time Data Display

The use of a fast microcomputer, such as an IBM Personal Computer with a hard disk and programs written in assembly language for data acquisition and display, would allow the real

time display of data. The temperatures of all 16 thermocouples could then be displayed simultaneously on the screen in a four by four window matrix as they are acquired. In this way, the early detection of air bubbles and other error conditions would be possible.

### 5.2.4. Hardware Suggestions

Extensive modification of the existing hardwave (e.g., building a new phantom) is both expensive and time consuming. However, the effects of the reflections and the partially degassed water can be overcome. Sound absorbing material of high quality and in high volume could be used to line the walls of the water tank in which the phantom is submerged. Experiments need to be performed in such a way as to minimize the effect at the walls of the phantom. If phantom regions with high reflections must be used, then the effects of the Plexiglas reflections need be accounted for or else erroneous results will be produced. Finally, degassed water of the highest quality available needs to be used at all times. For best results, a test for dissolved oxygen should be performed on the water to be used. The implementation of these suggestions should greatly improve the operating characteristics of the acoustic tissue phantom so that it can be effectively used to measure the performance of ultrasonic hyperthermia applicators.

# TABLES

Table 2.1. Acoustic Properties of Phantom Material Mixture.

| Frequency MHz | Attenuation Coefficient in dB/cm | Propagation Velocity of Sound m/sec |
|---|---|---|
| 1.00 | 0.65 (estimated) | 1544 (estimated) |
| 1.20 | 0.75 | 1544 |
| 2.50 | 1.39 | 1544 |
| 4.50 | 2.42 | 1544 |

Table 3.1. First 20 Temperature Data Points Used for the Calculation of the Specific Heat.

| Time Sec | Recorded Temperature $^{o}C$ | Time Sec | Recorded Temperature $^{o}C$ |
|---|---|---|---|
| 0 | -0.02 | 12 | 0.38 |
| 2 | -0.02 | 14 | 0.57 |
| 4 | -0.03 | 16 | 0.92 |
| 6 | -0.03 | 18 | 1.04 |
| 8 | -0.03 | 20 | 1.40 |
| 10 | -0.03 | 22 | 1.61 |

Table 3.2. Power Deposition in $W/cm^3$, Set A.

| | Bus Number | | | |
|---|---|---|---|---|
| Position | 4 | 3 | 2 | 1 |
| D | 0.30 | 0.14 | 0.17 | 0.16 |
| C | 0.14 | 0.10 | 0.19 | 0.15 |
| B | 0.14 | 0.13 | 0.17 | 0.15 |
| A | 0.19 | 0.25 | 0.21 | 0.19 |

Table 3.3. Temperatures Reached at 60 sec, Set A.

| | Bus Number | | | |
|---|---|---|---|---|
| Position | 4 | 3 | 2 | 1 |
| D | 1.2 | 0.85 | 1.15 | 0.9 |
| C | 0.5 | 0.85 | 0.75 | 0.45 |
| B | 1.25 | 0.60 | 0.40 | 0.45 |
| A | 0.75 | 0.80 | 0.55 | 0.50 |

Table 3.4. Power Deposition in $W/cm^3$, Set B.

| | Bus Number | | | |
|---|---|---|---|---|
| Position | 4 | 3 | 2 | 1 |
| D | 0.21 | 0.10 | 0.22 | 0.12 |
| C | 0.12 | 0.09 | 0.15 | 0.06 |
| B | 0.15 | 0.08 | 0.12 | 0.07 |
| A | 0.11 | 0.20 | 0.10 | 0.05 |

Table 3.5. Temperatures Reached at 60 sec, Set B.

| | Bus Number | | | |
|---|---|---|---|---|
| Position | 4 | 3 | 2 | 1 |
| D | 2.15 | 1.50 | 2.45 | 1.65 |
| C | 1.90 | 0.95 | 1.55 | 1.15 |
| B | 2.90 | 1.15 | 0.95 | 0.65 |
| A | 1.50 | 2.25 | 1.10 | 0.40 |

Table 3.6. Power Deposition in $W/cm^3$, Set C.

| | Bus Number | | | |
|---|---|---|---|---|
| Position | 4 | 3 | 2 | 1 |
| D | 0.32 | 0.15 | 0.18 | 0.14 |
| C | 0.19 | 0.10 | 0.25 | 0.14 |
| B | 0.12 | 0.16 | 0.23 | 0.19 |
| A | 0.14 | 0.27 | 0.11 | 0.24 |

Table 3.7. Temperatures Reached at 60 sec, Set C.

| | Bus Number | | | |
|---|---|---|---|---|
| Position | 4 | 3 | 2 | 1 |
| D | 3.8 | 2.3 | 2.3 | 2.4 |
| C | 9.7 | 1.5 | 2.4 | 2.0 |
| B | 2.5 | 2.2 | 3.5 | 3.2 |
| A | 2.3 | 3.5 | 2.7 | 3.2 |

Table 3.8. Power Deposition at 1 cm (Bus No. 7), 2 cm (Buses Nos. 4 and 1), and 5 cm (Bus No. 5).

| | Bus Number | | | |
|---|---|---|---|---|
| Position | 7 | 4 | 1 | 5 |
| D | 0.12 | 0.12 | 0.27 | 0.15 |
| C | 0.15 | 0.16 | 0.13 | 0.10 |
| B | 0.18 | 0.19 | 0.18 | 0.15 |
| A | 0.18 | 0.19 | 0.15 | 0.1 |

Table 3.9. Temperatures Reached at 60 sec at 1 cm (Bus No. 7), 2 cm (Buses Nos. 4 and 1), and 5 cm (Bus No. 5).

| | Bus Number | | | |
|---|---|---|---|---|
| Position | 7 | 4 | 1 | 5 |
| D | 1.99 | 1.71 | 3.63 | 2.53 |
| C | 2.46 | 2.38 | 1.81 | 1.32 |
| B | 2.47 | 2.42 | 2.74 | 2.06 |
| A | 2.88 | 2.81 | 1.78 | 1.28 |

Table 3.10. Incident Power and Theoretical Absorbed Power at 0, 1, 2, and 5 cm.

| Depth cm | Incident Power at Indicated Depth | Theoretical Absorbed Power in $W/cm^3$ at Indicated Depth |
|---|---|---|
| 0 | 3.27 | 0 |
| 1 | 2.82 | 0.42 |
| 2 | 2.42 | 0.36 |
| 5 | 1.55 | 0.23 |

Table 3.11. Comparison of Data in Tables 3.8 and 3.10.

| Depth cm | Average Power Deposited (Table 3.8) $W/cm^3$ | Calculated Absorbed Power (Table 3.10) $W/cm^3$ | Scattered Power % |
|---|---|---|---|
| 1 | 0.16 | 0.42 | 62% |
| 2 | 0.17 | 0.36 | 53% |
| 5 | 0.13 | 0.23 | 46% |

Table 3.12. Power Deposition Due to the Outer 12 Elements.

| | Bus Number | | | |
|---|---|---|---|---|
| Position | 4 | 3 | 2 | 1 |
| A | 0.16 | 0.13 | 0.10 | 0.06 |
| B | 0.11 | (0.03) | (0.03) | 0.05 |
| C | 0.07 | (0.03) | (0.03) | 0.06 |
| D | 0.20 | 0.06 | 0.07 | 0.21 |

Table 3.13. Temperatures Reached at 180 sec Due to the Outer 12 Elements.

| | Bus Number | | | |
|---|---|---|---|---|
| Position | 4 | 3 | 2 | 1 |
| A | 3.92 | 3.59 | 2.45 | 2.71 |
| B | 4.18 | 0.73 | 0.73 | 3.08 |
| C | 2.75 | 0.84 | 0.77 | 2.97 |
| D | 4.43 | 2.82 | 2.31 | 4.17 |

Table 3.14. Power Deposition Due to the Inner Four Elements.

| | Bus Number | | | |
|---|---|---|---|---|
| Position | 4 | 3 | 2 | 1 |
| A | -- | -- | -- | -- |
| B | -- | 0.07 | 0.10 | -- |
| C | -- | 0.07 | 0.12 | -- |
| D | -- | -- | -- | -- |

Table 3.15. Temperatures Reached at 180 sec Due to the Inner Four Elements.

| | Bus Number | | | |
|---|---|---|---|---|
| Position | 4 | 3 | 2 | 1 |
| A | 0.17 | 0.38 | 0.38 | 0.18 |
| B | 0.29 | 1.63 | 1.97 | 0.34 |
| C | 0.26 | 1.71 | 1.84 | 0.28 |
| D | 0.15 | 0.31 | 0.22 | 0.15 |

Table 3.16. A Comparison of Actual Data and Simulated Noise Ridden Data.

| Time in sec | Actual Temperature $^{o}C$ | Sampled Temperature $^{o}C$ |
|---|---|---|
| 10 (0) | 0.0 | 0.0 |
| 12 | 0.1 | 0.165 |
| 14 | 0.2 | 0.1 |
| 16 | 0.3 | 0.34 |
| 18 | 0.4 | 0.43 |
| 20 (10) | 0.5 | 0.43 |

Slope resulting from curve fitting = $0.0455^{o}C/sec$

Table 4.1. Percentage of Scattered Power.

| Data Source | Power Deposited $W/cm^3$ | Power Attenuated $W/cm^3$ | Percentage Power Scattered $W/cm^3$ |
|---|---|---|---|
| Table 3.2 | 0.17 | 0.3 | 43% |
| Table 3.4 | 0.12 | 0.45 | 73% |
| Table 3.6 | 0.18 | 0.45 | 60% |

# FIGURES

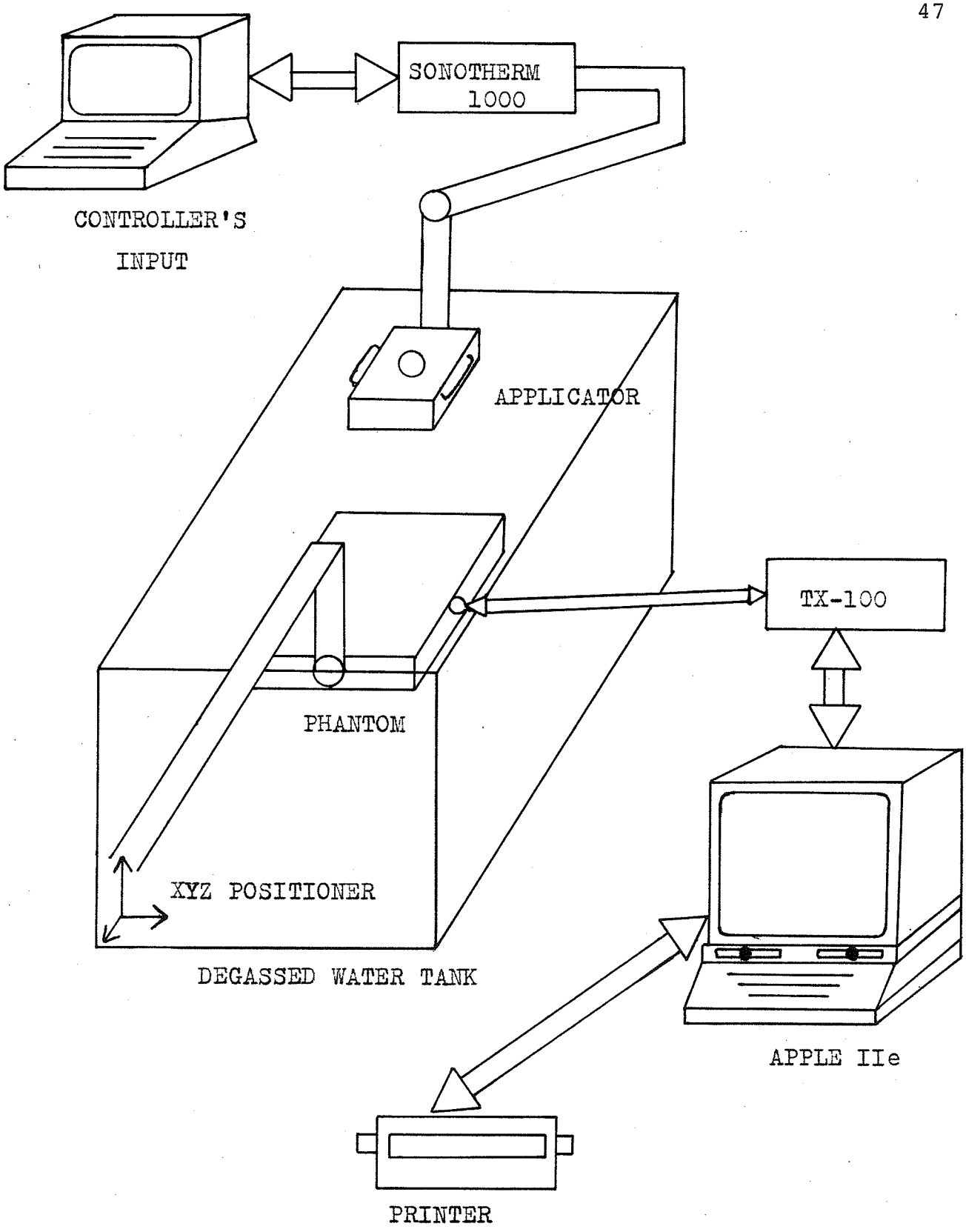


Figure 2.1. Equipment interconnection for data acquisition.

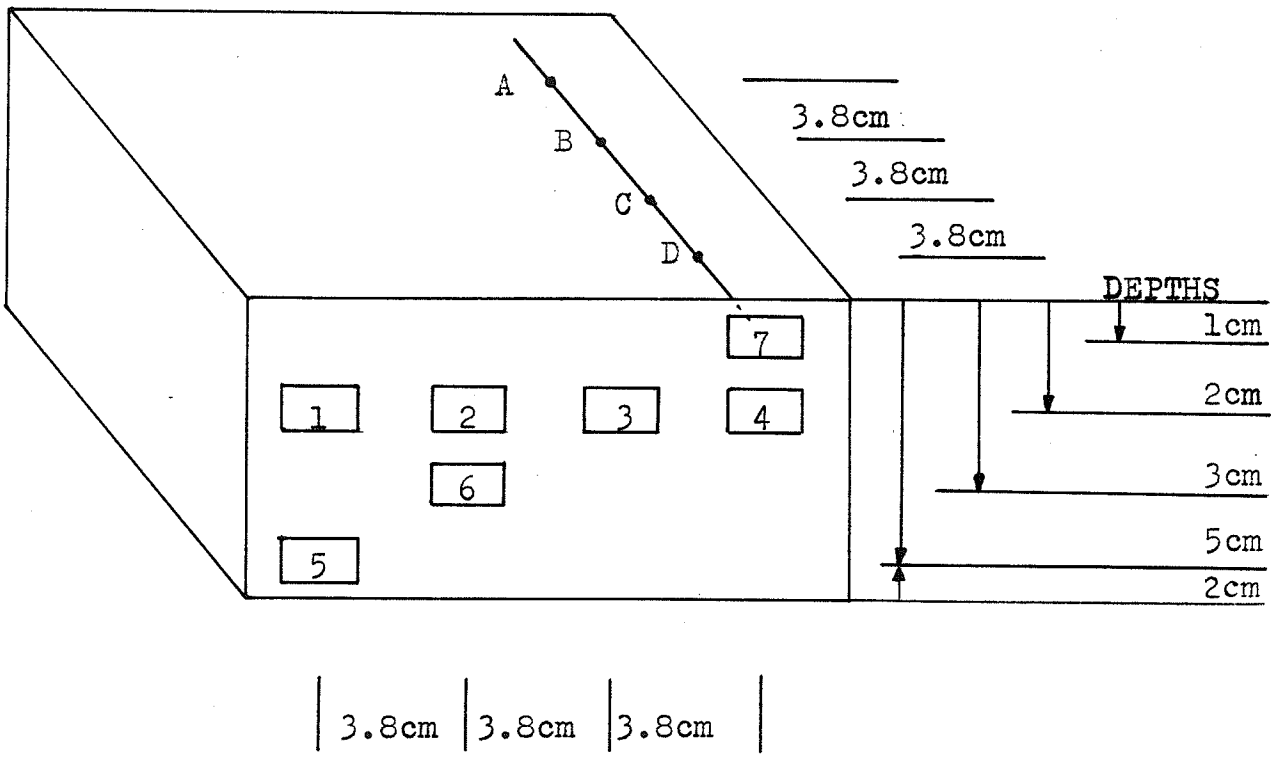


Figure 2.2. Thermocouples cubic lattice arrangement.

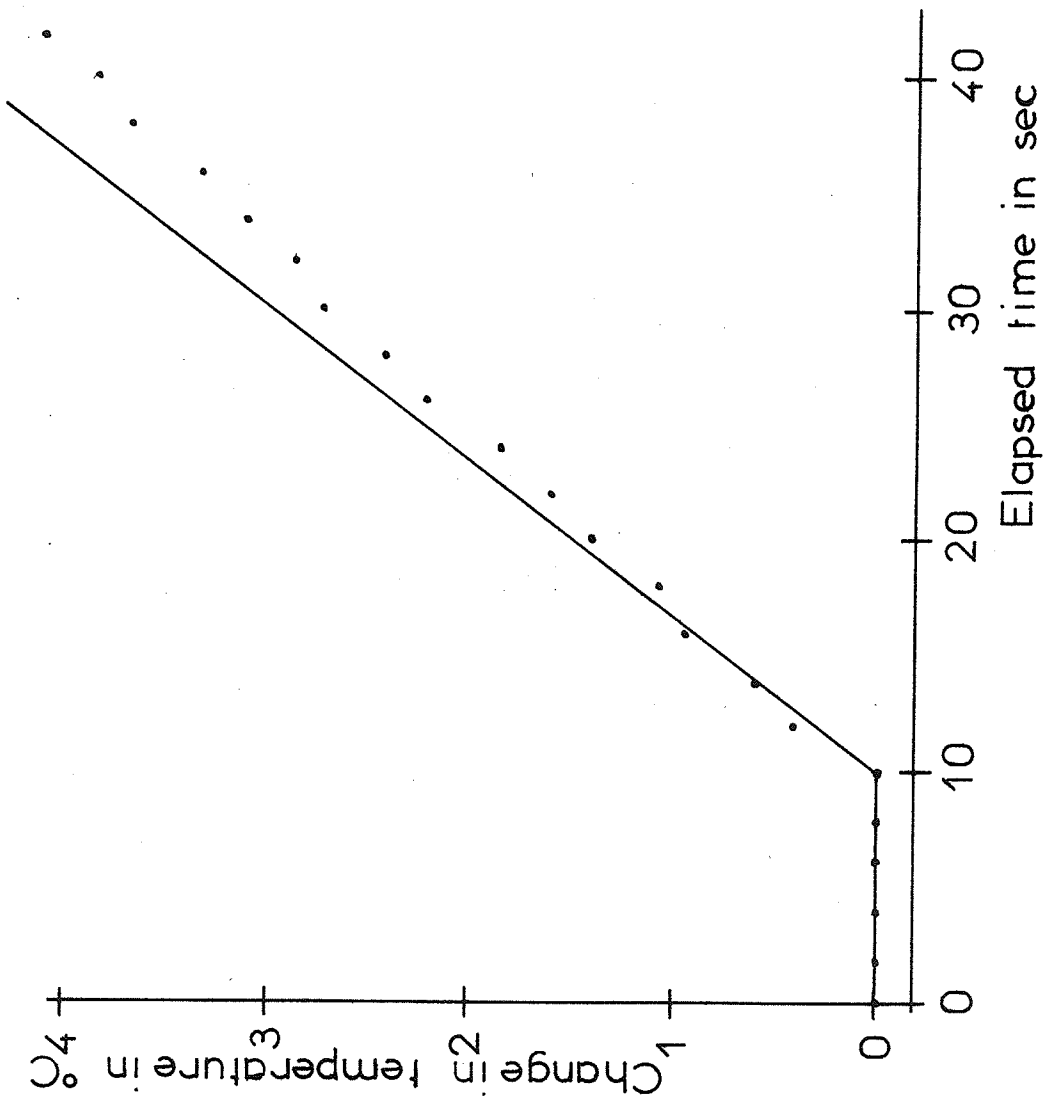


Figure 3.1. Temperature versus time plot for the specific heat calculation.

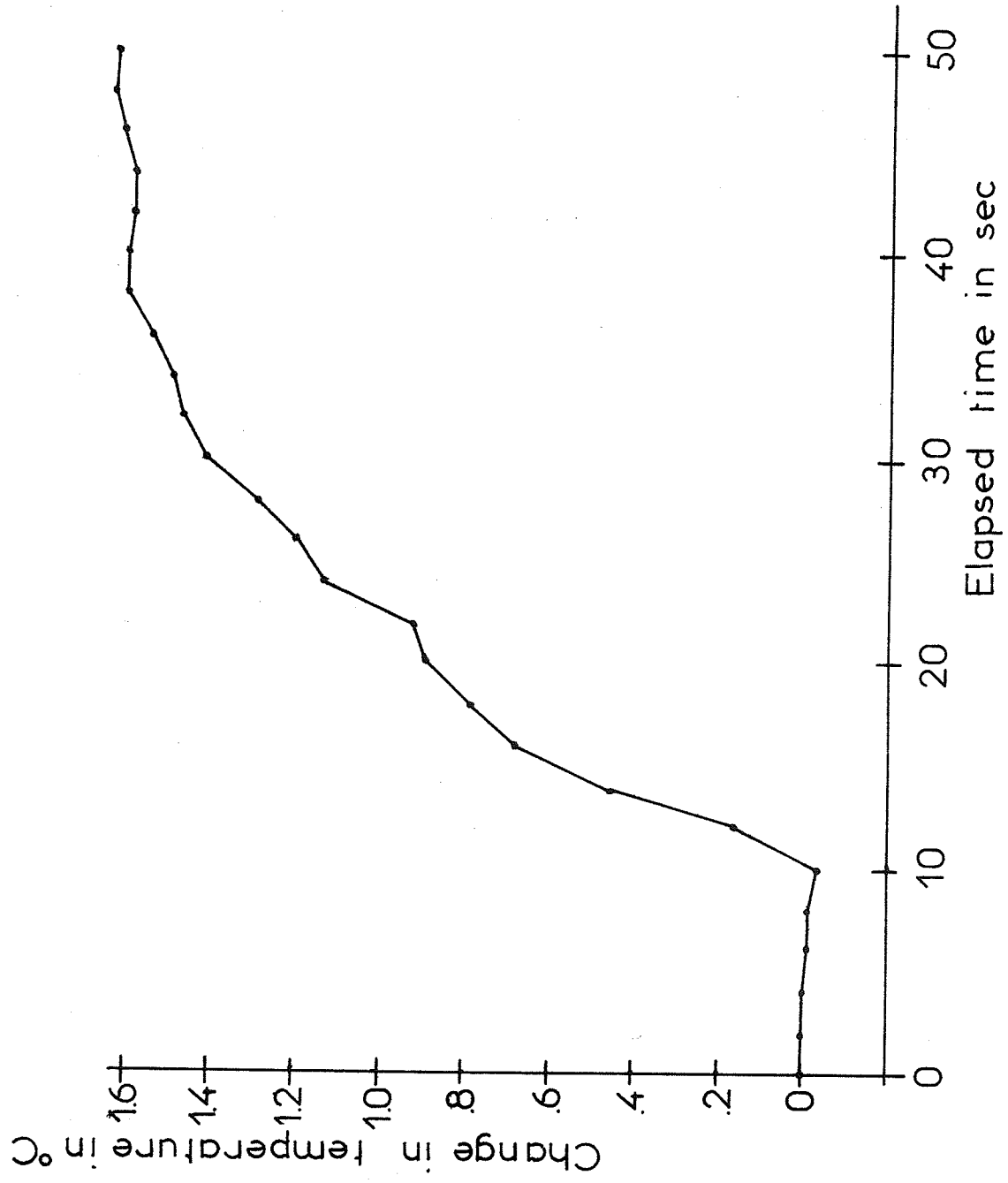


Figure 3.2. Typical temperature versus time plot.

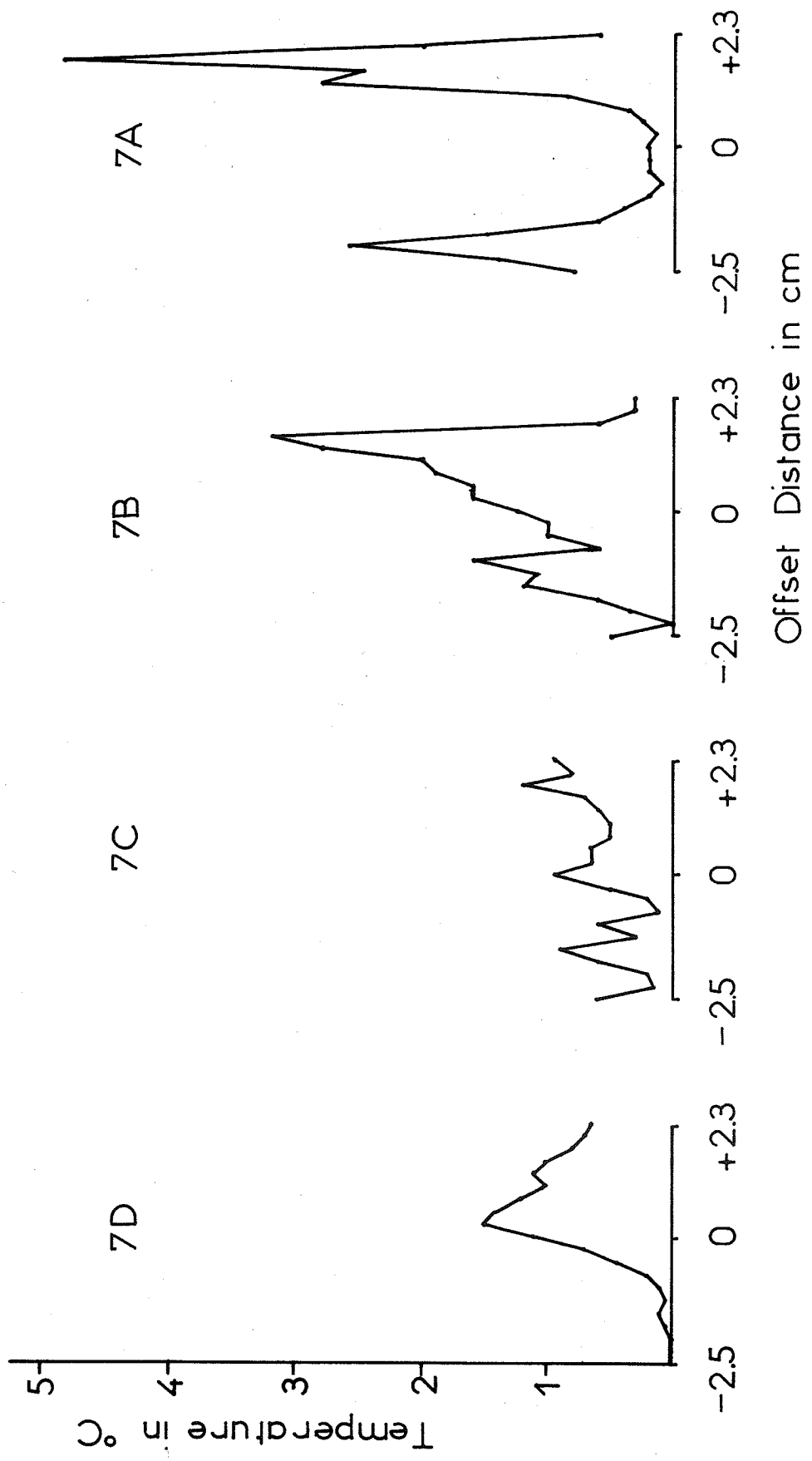


Figure 3.3. Beam plots of 7D, 7C, 7B, 7A, at 1 cm.

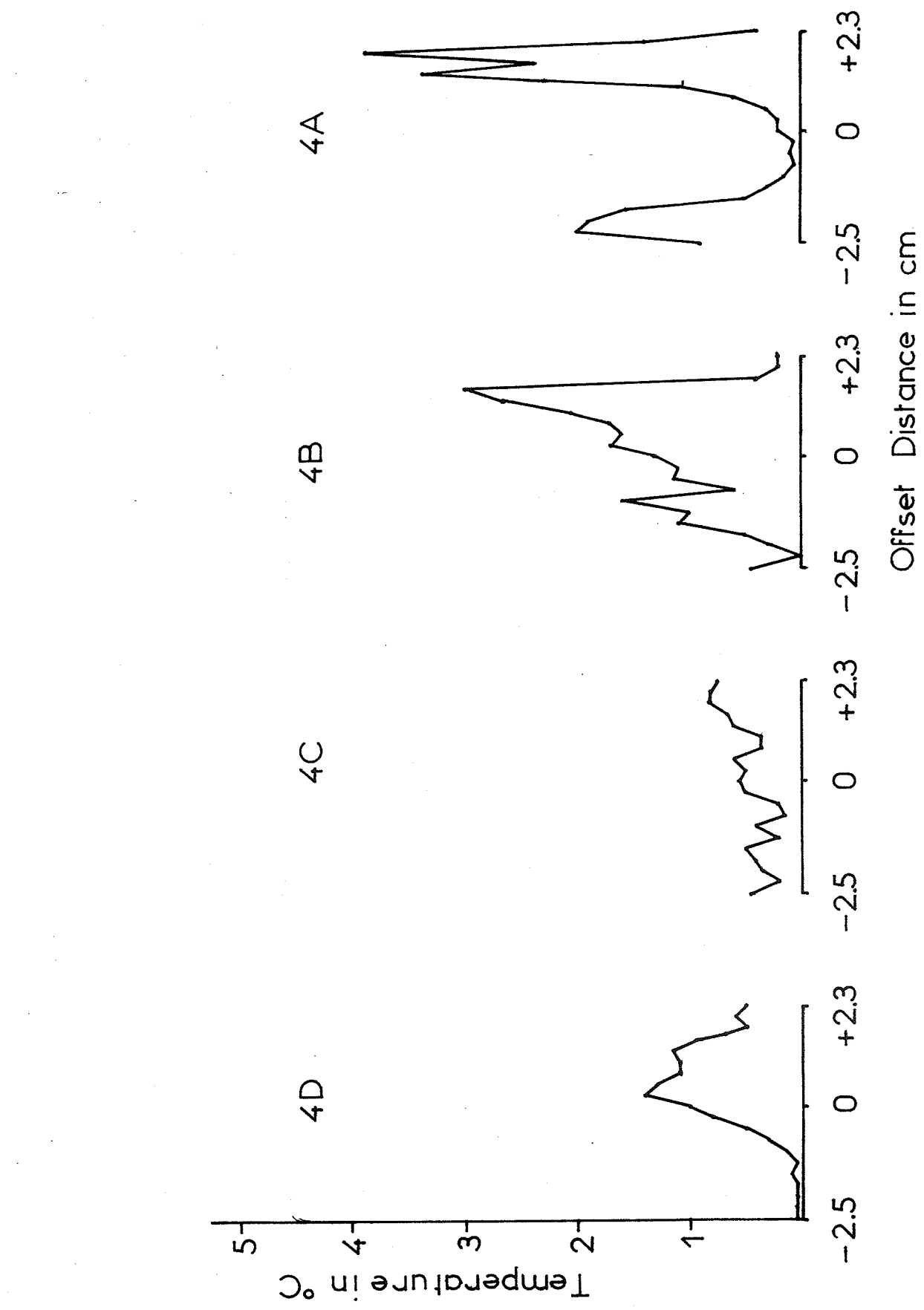


Figure 3.4. Beam plots of 4D, 4C, 4B, 4A at 2 cm.

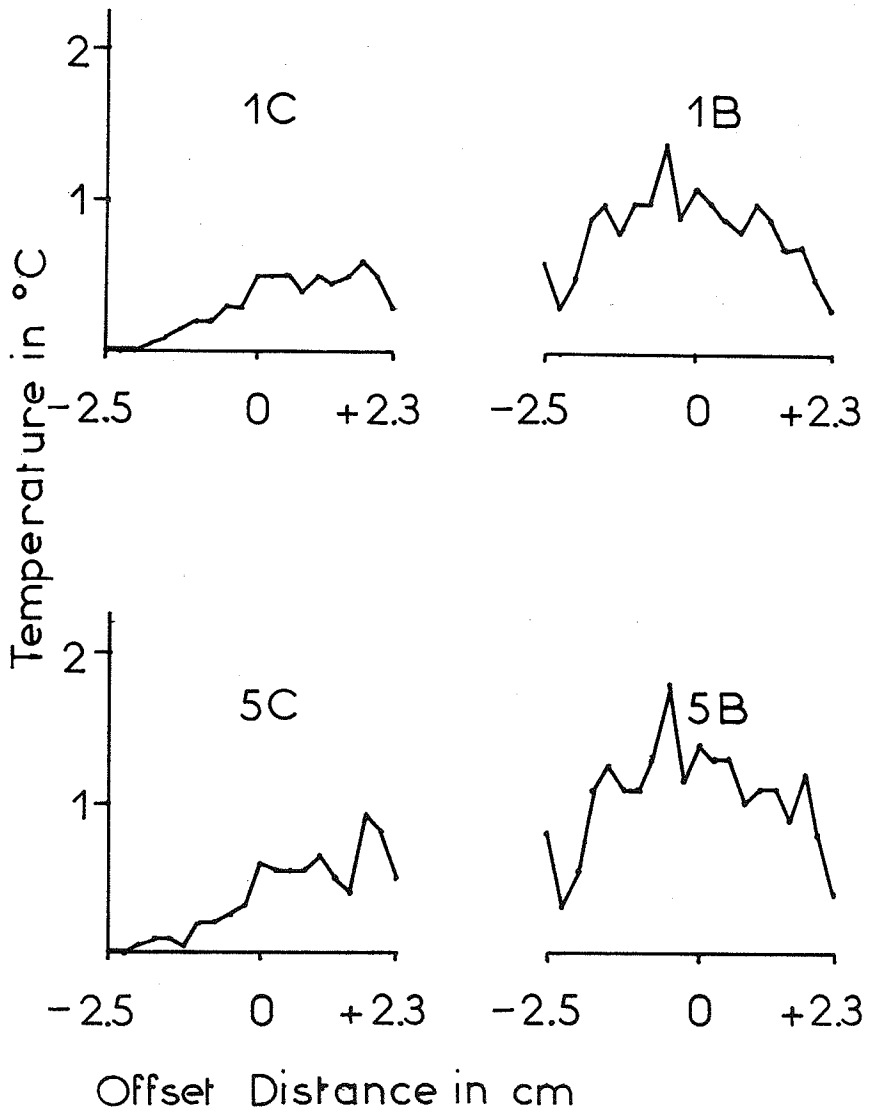


Figure 3.5. Beam plots of 1C, 1B and 5C, 5B at 2 and 5 cm.

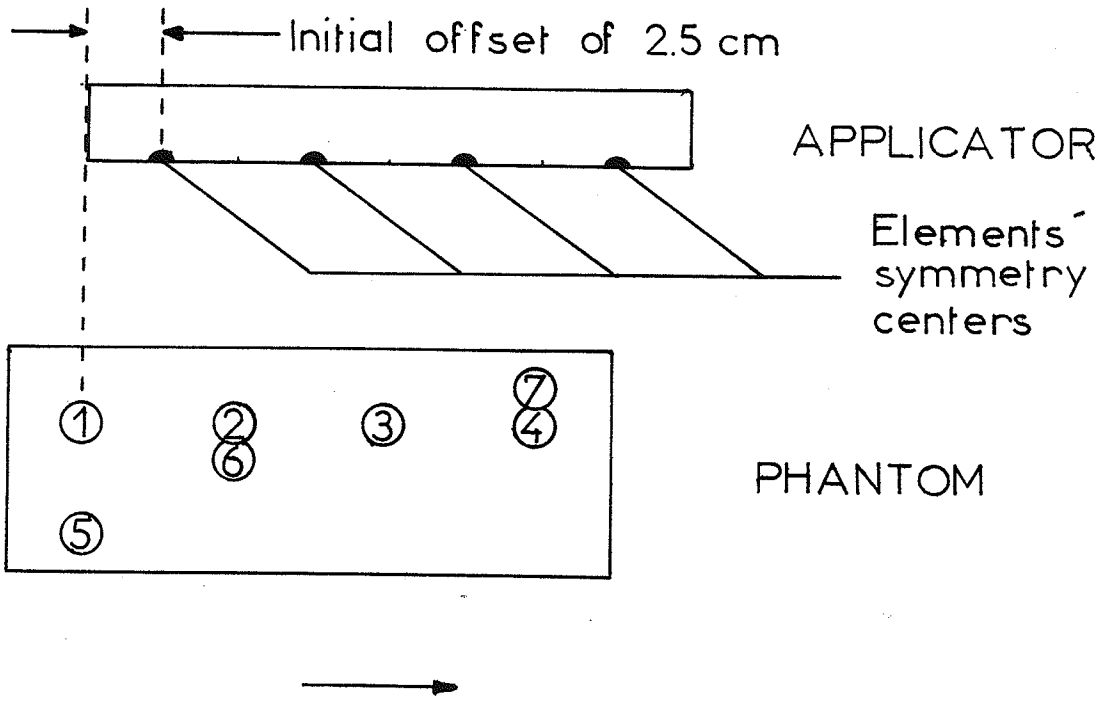


Figure 3.6. Offset distance set up for beam plots.

File: A15M85

Elements On: All

Power On For: 60 sec

Thermocouple Buses Monitored: No. 1, 2, 3, 4

Depth(s): 2 cm

Incident power per $cm^2$: 2.69 $W/cm^2$

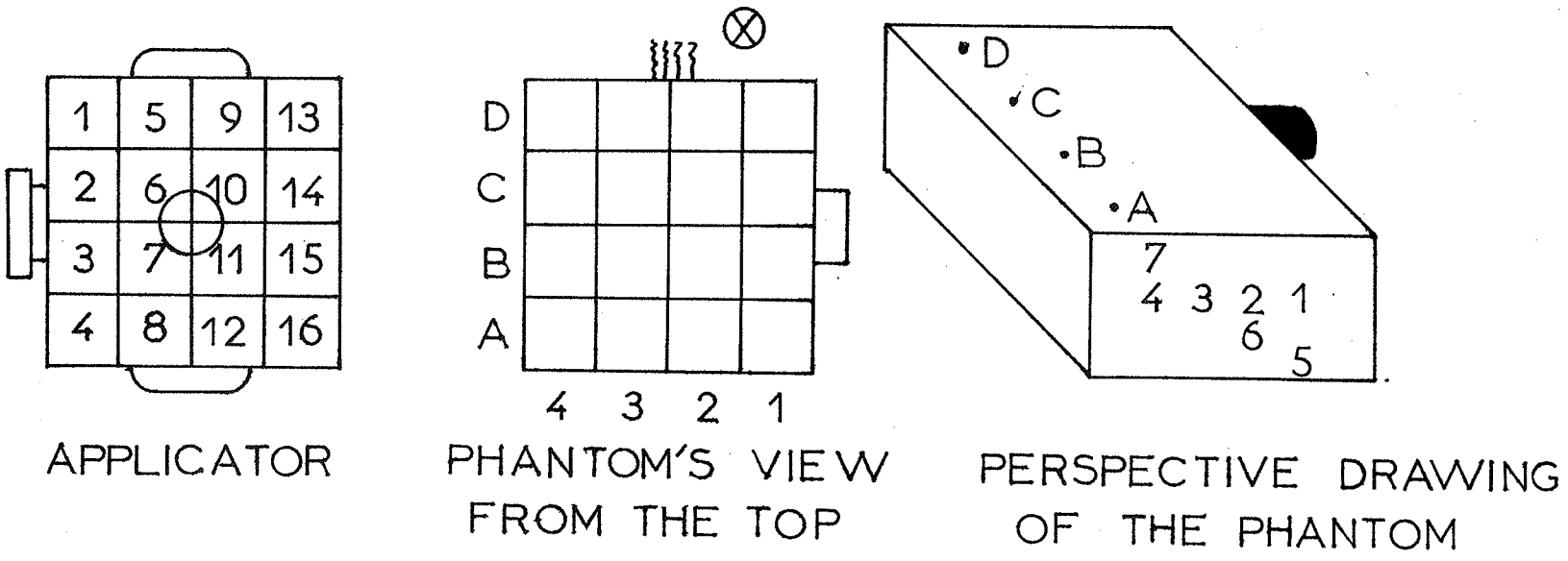


Figure 3.7. Data and set up for data set A.

File: B15M85

Elements On: All

Power On For: 60 sec

Thermocouple Buses Monitored: No. 1, 2, 3, 4

Depth(s): 2 cm

Incident power per $cm^2$: 4.04 $W/cm^2$

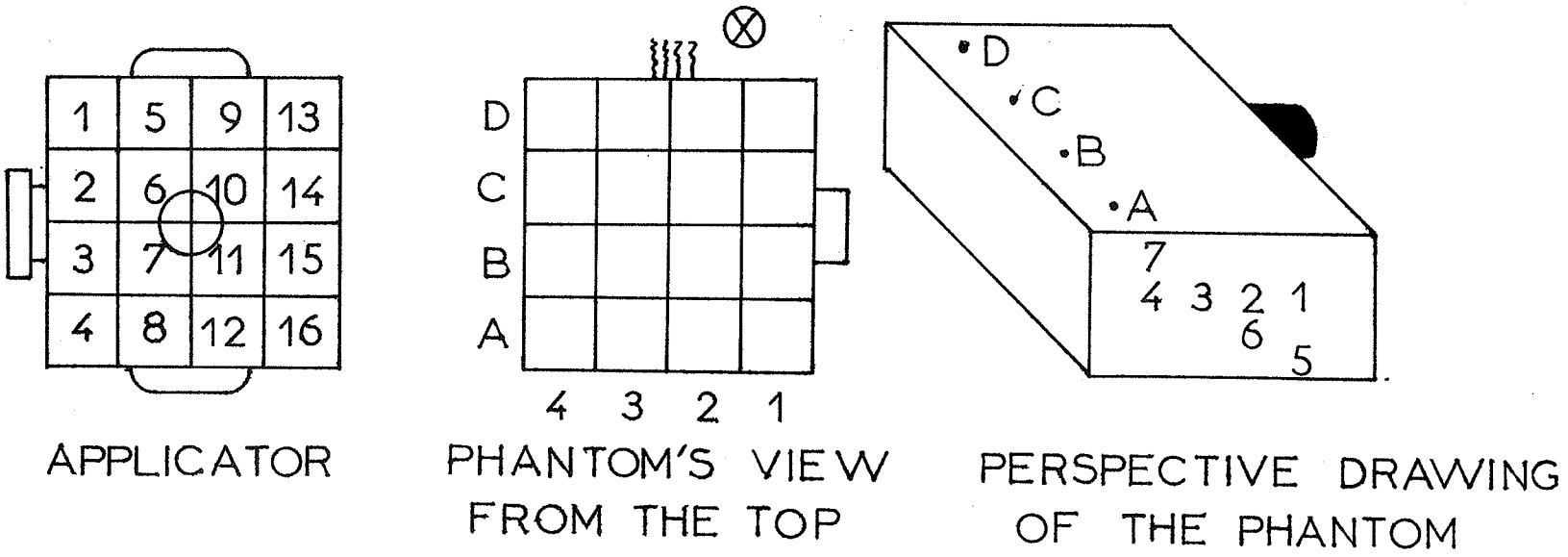


Figure 3.8. Data and set up for data set B.

File: C15M85

Elements On: All

Power On For: 60 sec

Thermocouple Buses Monitored: No. 1, 2, 3, 4

Depth(s): 2 cm

Incident power per $cm^2$: 4.04 $W/cm^2$

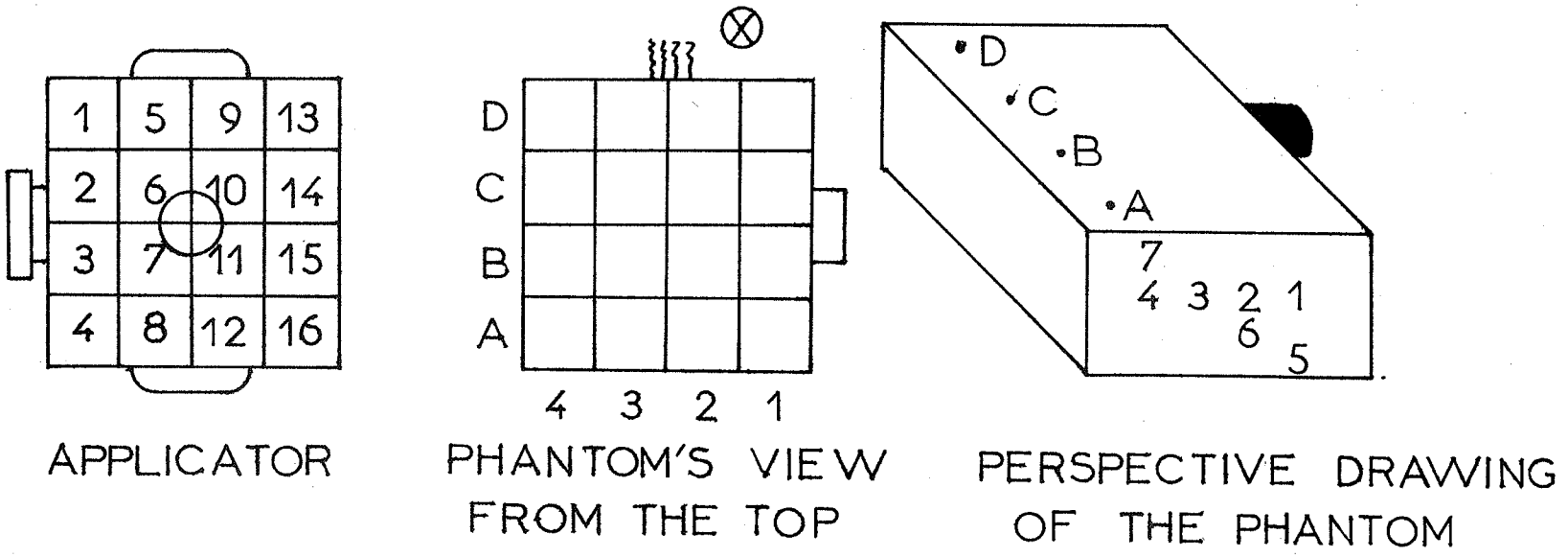


Figure 3.9. Data and set up for data set C.

File: D15M85

Elements On: All

Power On For: 60 sec

Thermocouple Buses Monitored: No. 7, 4, 1, 5

Depth(s): Bus No. 7 at 1 cm, Buses No. 4 and 1 at 2 cm, Bus No. 5 at 5 cm

Incident power per $cm^2$: 3.27 $W/cm^2$

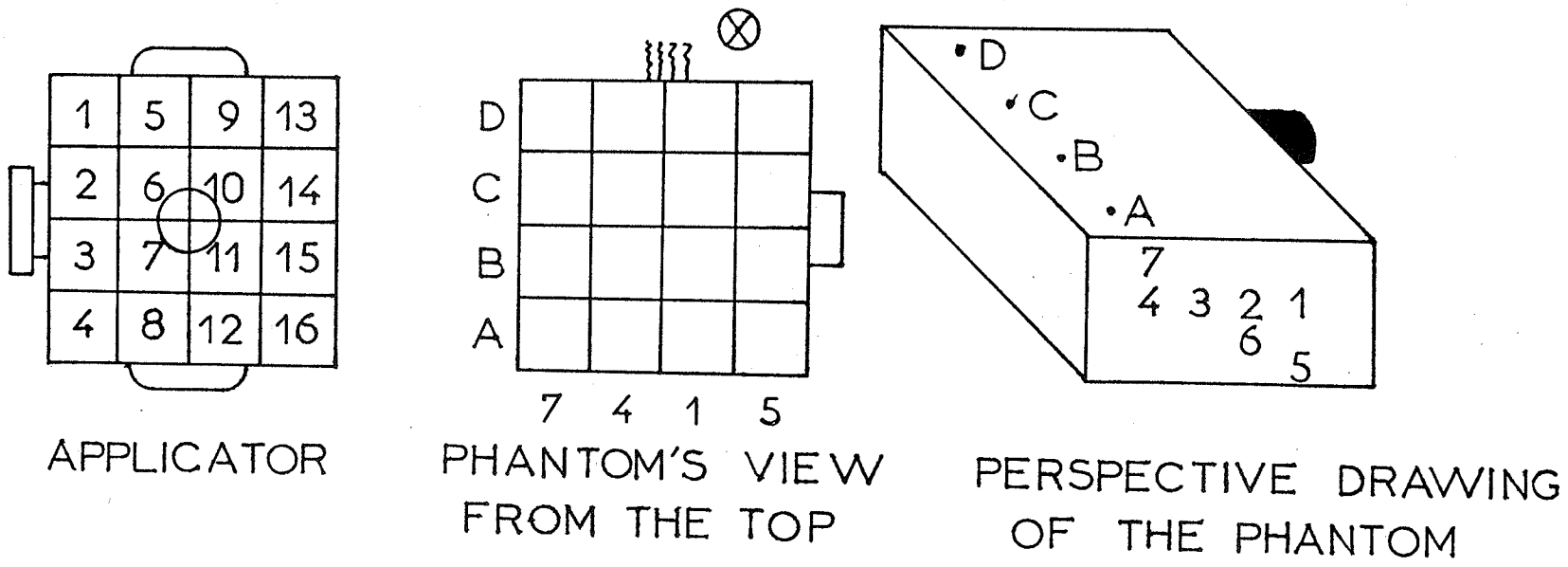


Figure 3.10. Data and set up for depths at 1, 2, and 5 cm.

File: H15M85

Elements On: Outer 12; 1, 2, 3, 4, 5, 8, 9, 12, 13, 14, 15, 16

Power On For: 180 sec

Thermocouple Buses Monitored: No. 1, 2, 3, 4

Depth(s): 5 cm

Incident power per $cm^2$: 3.34 $W/cm^2$

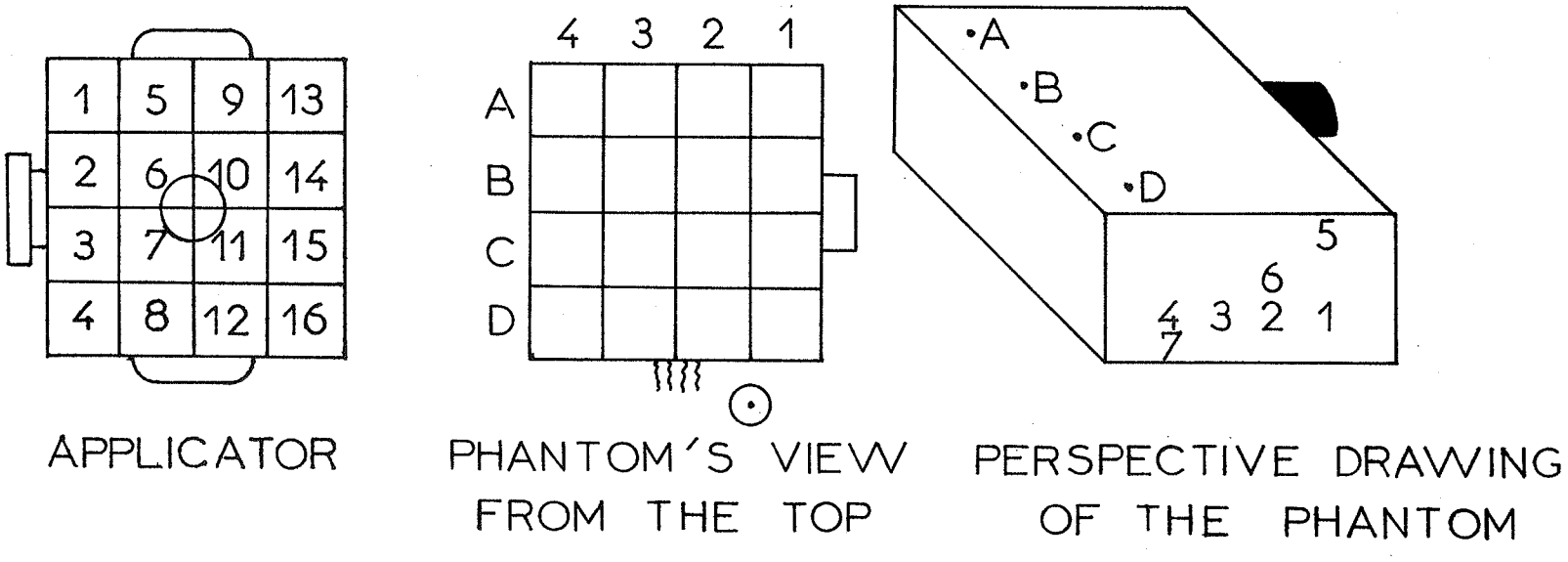


Figure 3.11. Data and set up for outer 12 elements.

File: A16M85

Elements On: Center 4; 6, 7, 10, 11

Power On For: 180 sec

Thermocouple Buses Monitored: 1, 2, 3, 4

Depth(s): 5 cm

Incident power per $cm^2$: 3.49 $W/cm^2$

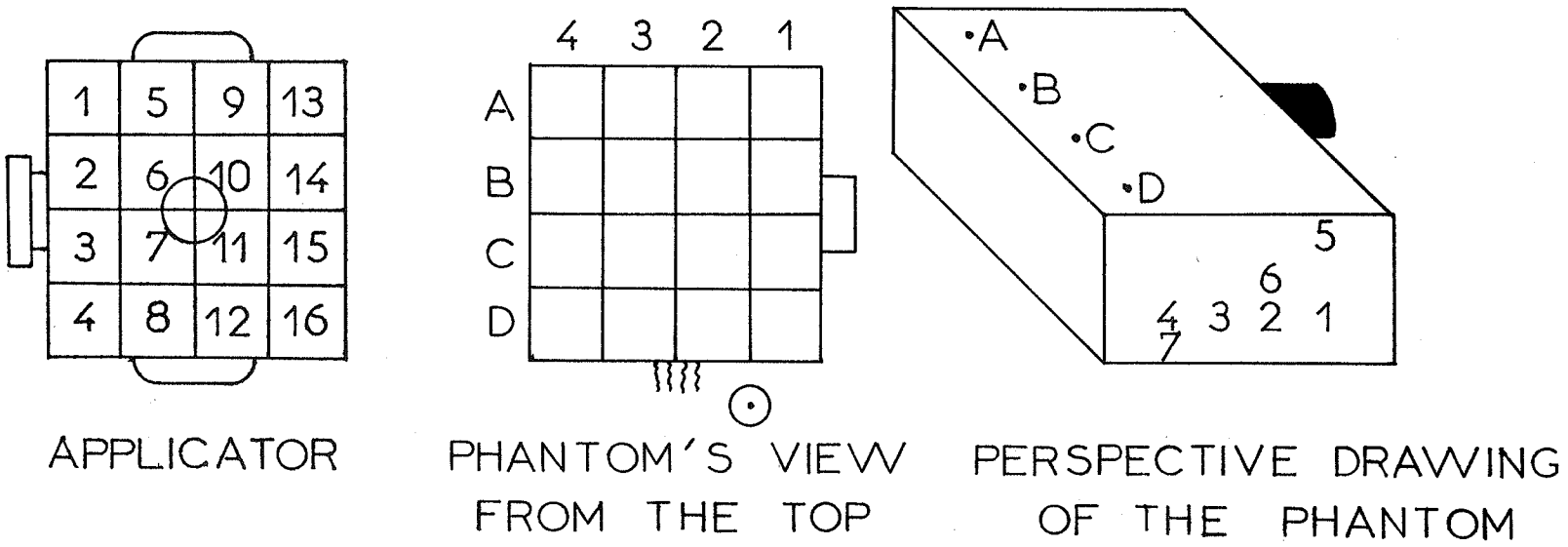


Figure 3.12. Data and set up for inner 4 elements.

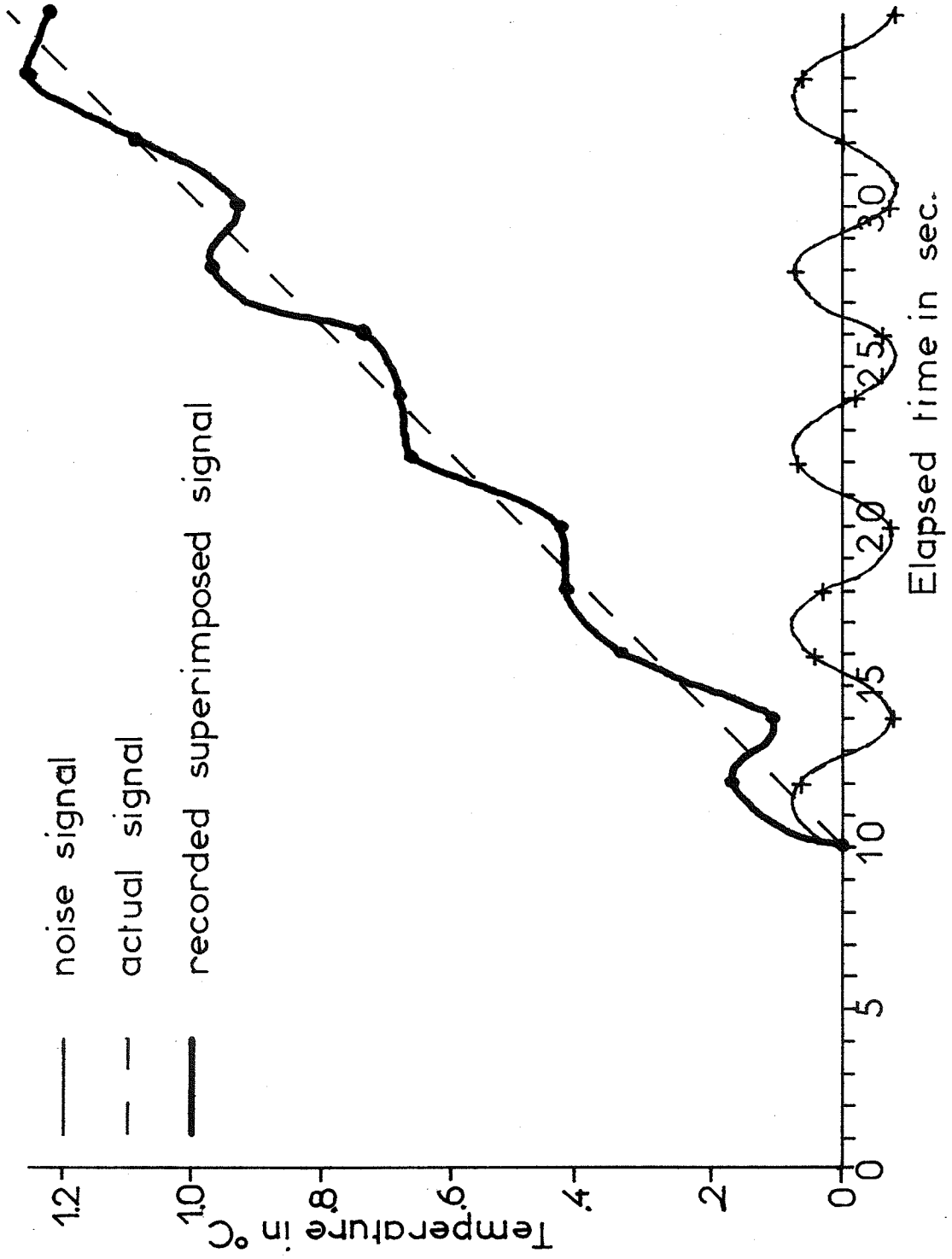


Figure 3.13. Noise ridden data (superimposed signal).

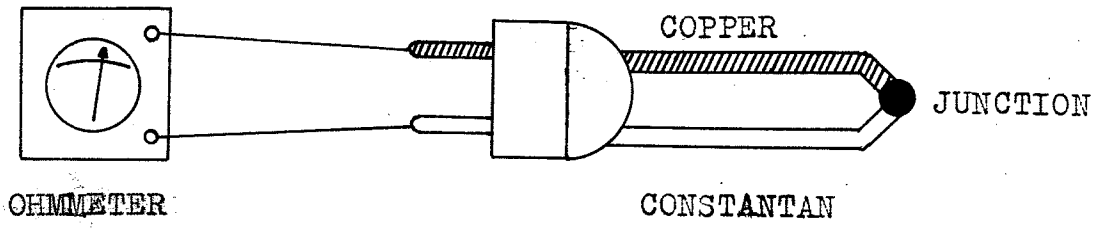


PHYSICAL CIRCUIT

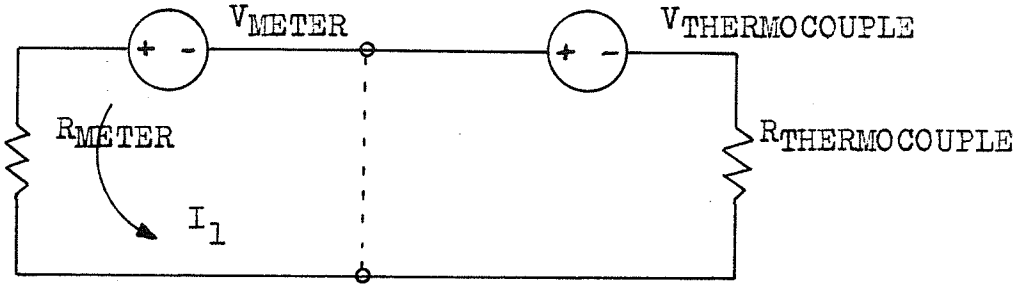


EQUIVALENT CIRCUIT #1

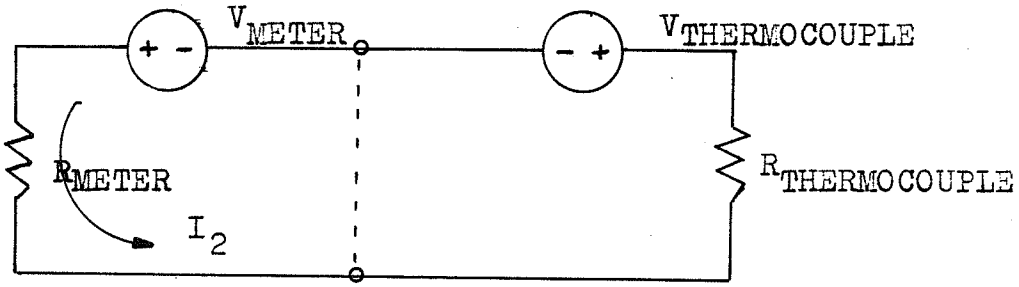


EQUIVALENT CIRCUIT #2

$$I_1 = \frac{V_{METER} + V_{THERMOCOUPLE}}{R_{METER} + R_{THERMOCOUPLE}}$$

$$I_2 = \frac{V_{METER} - V_{THERMOCOUPLE}}{R_{METER} + R_{THERMOCOUPLE}}$$

$I_1 \neq I_2$ $\therefore$ (ERRONEOUSLY) $R_{THERMOCOUPLE\#1} \neq R_{THERMOCOUPLE\#2}$

Figure 3.14. Error source of thermocouple resistance value.

# REFERENCES

Bertino, J. R., Kowal, C. D., Klein, M. E., Docbrowski, J., and Mini, E. "The Potential for Chemotherapy and Hyperthermia," Front. Radia. Ther. Oncol. 18:162-170, Karger, Basel 1984.

Bowman, H. F., Cravalho, E. G., and Woods, M. "Theory, Measurement, and Application of Thermal Properties of Biomaterials," Ann. Review of Biophysics and Bioengineering, Vol. 4, pp. 43-80, 1975.

Cetas, T. C. "The Philosophy and Use of Tissue-equivalent Electromagnetic Phantoms," Physical Aspects of Hyperthermia American Assoc. Physicists in Medicine, Medical Physics Monograph No. 8, 1982.

Hahn, G. M. "Hyperthermia and Cancer," New York and London, Plenum Press, 1982.

Iskander, M. F. "Physical Aspects and Methods of Hyperthermia Production by RF Currents and MW," American Assoc. of Physicists in Medicine, Medical Physics Monograph No. 8, 1982.

Lele, R. P. "Physical Aspects and Clinical Studies with Ultrasonic Hyperthermia," Ch. 16 in F. K. Storm, ed. "Hyperthermia in Cancer Therapy," Boston, Hall G. K. 1983.

Padgitt, D. G. "An Ultrasonic Transducer Field Scanner System," M.S. Thesis, University of Illinois, Urbana-Champaign, IL, 1984.

Repacholi, M. H. "Ultrasound: Characteristics and Biological Action," National Research Council of Canada, Publ. No.

19244, 1981.

Separato, S. A. "The Biology of Hyperthermia in Vitro," American Association of Physicists in Medicine, Medical Physics Monograph, No. 8, 1982.

Separato, S. A., Rapphorst, G., and Dewey, W. C. "Cell Killing and Sequencing of Hyperthermia and Radiation," Int. J. Radiat. Oncol. Biol. Phys. 1979, 5:343-347.

Storm, F. K., ed. "Hyperthermia in Cancer Therapy," Boston, Hall G. K. 1983.

Underwood, H. R. "Field Characteristics of a Multielement Ultrasonic Transducer Applicator for Hyperthermia Therapy," M.S. Thesis, University of Illinois, Urbana-Champaign, Urbana, IL 1986.

# University of Illinois at Urbana-Champaign

DEPARTMENTAL FORMAT APPROVAL

THIS IS TO CERTIFY THAT THE FORMAT AND QUALITY OF PRESENTATION OF THE THESIS SUBMITTED BY PANAYIOTIS HADJIMITSOS AS ONE OF THE REQUIREMENTS FOR THE DEGREE OF MASTER OF SCIENCE IS ACCEPTABLE TO THE DEPARTMENT OF ELECTRICAL AND COMPUTER ENGINEERING.

*(Full Name of Department, Division or Unit)*

13 August 1986

*Date of Approval*

*Departmental Representative*